# Analysis of a coherent 3D imaging sensor for long-range LiDAR

*Preethi Padmanabhan*, Steven Fortune, Andres Forrer, Fabiana Settembrini, and Remus Nicolaescu*
*Pointcloud GmbH, Zürich, Switzerland, *E-Mail: preethi.padmanabhan@ieee.org*

***Abstract*—This paper presents the concepts and principles of coherent detection technology using analytical modeling. System level comparisons are made with a direct detection technology, namely, dToF and important performance metrics such as SNR and detection probability are derived. The analysis particularly demonstrates the suitability of coherent imaging for long range LiDAR scenarios. Additionally, measurement results in support of the analysis are also presented.**

**Keywords—3D imaging, coherent detection, LiDAR, system modeling**

## I. Introduction

Three-dimensional (3D) imaging has become a key enabling technology in a variety of applications in consumer, industrial, automotive and medical sectors. Most of these applications require at least one or more of the following conflicting requirements – long range, high signal-to-noise-ratio (SNR), high depth resolution/precision, high frame rate and low power consumption. Several 3D sensors exist that utilize direct-detection technologies for LiDAR applications [1,2]. However, many of the long-range commercial products today operate at high optical powers and/or with a scanning system to maximize the SNR [3]. Despite several noise-filtering techniques [4], the inherent nature of direct detection suffers due to low SNR especially in high ambient light.

Lately, 3D imaging technology based on coherent heterodyne detection using frequency-modulated continuous wave (FMCW) is becoming an increasingly popular alternative. The underlying principle makes it inherently insensitive to any incoherent background light, thus, making it very suitable for long-range, high-ambient light scenarios. Recently, a universal 3D imaging sensor on a Si-photonics platform measured up to 75m at ~4mW optical power, demonstrating the potential of this technology [5].

This paper presents the principles of a coherent heterodyne receiver with an analytical system model. Particularly, a long-range LiDAR application is explored for this work. Section II describes the analytical models for coherent imaging and direct detection pixels, particularly dToF. Simulations are presented for a typical outdoor LiDAR scenario and relevant system performance metrics, such as SNR and detection probability are estimated. Section III presents some characterization results including SNR and detection probability. Section IV finally concludes this work.

## II. Modeling and Analysis

### A. Analysis of coherent detection

A block diagram of a coherent heterodyne imaging pixel along with a timing diagram is shown below in Figure 1. A continuous-wave laser which is frequency modulated is used as the active source ($T_x$). A fraction of this is supplied as the local oscillator (LO) signal to the pixel. The scattered light from the target ($R_x$) is collected using grating couplers, optically mixed with the LO signal via a 50-50 directional coupler and detected by balanced photodetectors (PDs). A heterodyne current $i_b$, at the beat frequency $f_b$ corresponding to the target distance, is produced at the output of the PDs. This current is then amplified by a transimpedance amplifier (TIA) before being digitized for further processing with an ADC and DSP.

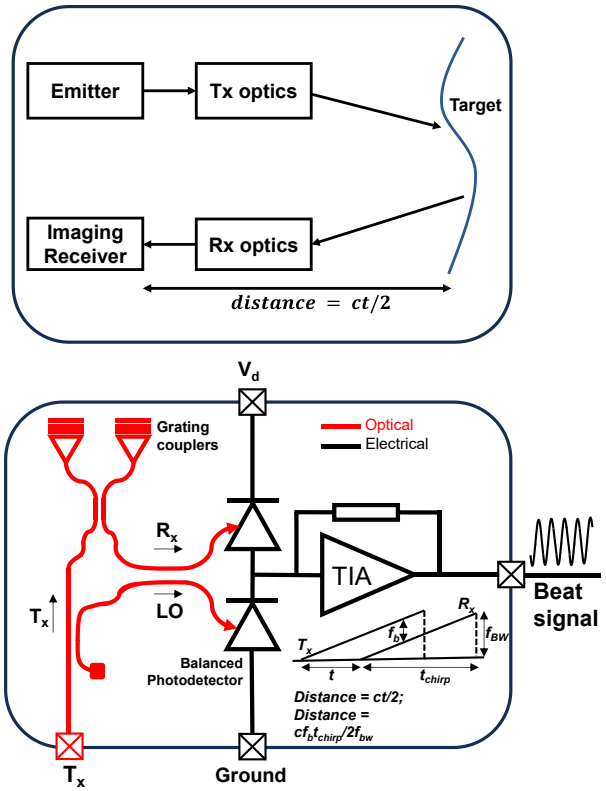


Figure 1- High-level LiDAR system components (top) and conceptual diagram of a coherent imaging pixel (bottom).

A heterodyne pixel can be modelled analytically and a first estimate of the system performance can be derived. For analysis purposes, a sawtooth frequency modulation scheme is used as shown above. The laser source is chirped linearly over a modulation bandwidth, $f_{BW}$ and integration time, $T_{chirp} = T_{int}$. The target distance, $d$, can then be deduced as follows:

$$d = \frac{ct}{2} = \frac{cf_b}{f_{bw}/T_{int}} \qquad \text{Equation 1}$$

For a given emitted optical power with a gaussian beam propagation, $P_{tx}$, the scattered power from the target, $P_{rx,coh}$, can be written as follows:

$$P_{rx,coh} = P_{tx} \times \rho \times \left(\frac{\lambda^2}{\pi w_d^2}\right) \times T_l \times T_{loss} \qquad \text{Equation 2}$$

where $\lambda$ is the laser wavelength, $\rho$ is the target reflectivity of a Lambertian circular target, $T_l$ is the lens efficiency and $T_{loss}$ accounts for any other optical loss in the path [6]. $w_d$ is the waist radius of the laser beam at the target at distance, $d$.
The heterodyne signal at the output of the PDs can then be written as follows:

$$I_{sig,coherent} = 2 \times R_{PD} \times \sqrt{P_{rx,coh} \times P_{LO}} \quad \text{Equation 3}$$

where $\sqrt{P_{rx,coh} \times P_{LO}}$ is the mixed optical output, $P_{LO}$ is the LO power and $R_{PD}$ is the responsivity of the PDs. In addition to the coherent target signal, shot noise, input referred TIA noise and ADC noise also contribute to the detected signal. Therefore, the total output signal at the PDs (and input of the analog front-end) becomes:

$$I_{out} = I_{sig,coherent} + I_{shot} + I_{TIA} + I_{ADC} \quad \text{Equation 4}$$

A coherent heterodyne pixel is typically operated in a shot-noise limited regime, in that, the LO shot noise is the dominant factor and other noise sources become negligible in comparison. An example simulation is shown in Figure 2 where the different noise sources are plotted.

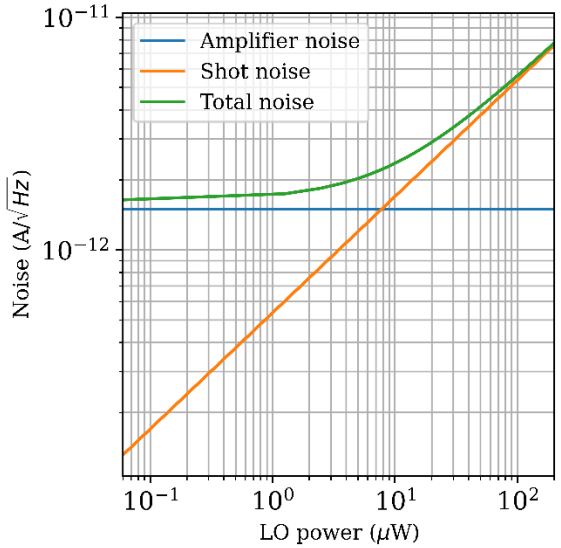


Figure 2- Noise analysis of a coherent heterodyne pixel.

It is seen that beyond ~10μW, shot noise starts to dominate and the one-sided power spectral density (PSD) in the shot noise limited regime can be approximated to the LO shot noise:

$$N_{shot} = 2qR_{PD}P_{LO} \quad \text{Equation 5}$$

Given the above assumption, the SNR can be derived from $I_{out}$ and $N_{shot}$ in Equations 4-5.

$$SNR = \frac{I_{out}^2 T_{int}}{2N_{shot}} \quad \text{Equation 6}$$

In order to get a quality depth measurement, SNR threshold, $SNR_{th}$, is usually applied to improve the detection probability while keeping the false detections minimal. For a given $SNR_{th}$, one can estimate the expected signal detection probability as follows:

$$P_{det} = \exp\left(-SNR_{th}/(1+SNR)\right) \quad \text{Equation 7}$$

The false detect probability, which is the probability that noise triggers a valid detection can be expressed as follows:

$$P_{fa} = \exp\left(-SNR_{th}\right) \quad \text{Equation 8}$$

It is important to notice that the SNR in the shot noise limited regime is basically independent of the LO power (see Equations 3-6). Despite that, the scattered target signal benefits from the optical amplification from the mixing operation at the pixel. Furthermore, Equation 2 shows that the only range-dependent factor in the scattered power is the beam radius, $w_d$. For a given beam size typically designed for the Rayleigh range, $R_{max}$, a coherent imaging pixel benefits from an almost constant $P_{rx}$ over the measurable range, as long as the divergence on the beam waist is not significant. Beyond this Rayleigh range, the SNR starts rolling off. This will be shown with supporting simulation results in Section III.
A direct detection technology is different, in that, the scattered light $P_{rx}$ decreases with the square of the target distance and SNR follows this behavior. In the next section, concepts of a direct detection based dToF pixel will be presented and analysed. Note that it is not in the scope of this paper to delve into the design details of a dToF pixel, but rather provide an example to analyze its differences with coherent detection.

### *B. Comparison with direct detection technology*

A dToF pixel typically consists of a single photon avalanche diode (SPAD) and a circuit such as a time-to-digital converter (TDC) to timestamp the photon arrival scattered from the target. An example dToF pixel in a start-stop configuration is shown in Figure 3 for this comparison. The target distance in a dToF pixel is derived directly in time domain as follows:

$$d = \frac{ct_{tof}}{2} \quad \text{Equation 9}$$

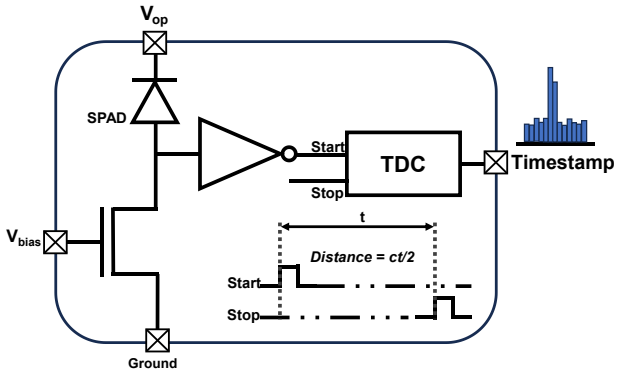


Figure 3- Conceptual diagram of a dToF pixel.

Performing a similar analysis as before, the signal and noise power for a dToF pixel will be derived. The scattered light $P_{rx}$ for a dToF pixel can be written as follows:

$$P_{rx,dToF} = P_{tx} \times \rho \times \left(\frac{D_{lens}^2}{4}\right) \times \frac{2}{\pi} \times T_l \times T_f \times \Delta_{BW} \times \frac{1}{d^2} \quad \text{Equation 10}$$

where $P_{tx}$ is the transmitted emitter power, $D_{lens}$ is the diameter of the lens, $T_f$ is the efficiency of the bandpass filter with passband $\Delta_{BW}$. One can notice the $1/d^2$ dependence of the scattered target signal, $P_{rx,dToF}$.
In an outdoor LiDAR, ambient light significantly contributes to noise. Other noise sources, such as the dark count rate (DCR) of the pixel, are often negligible compared to the ambient light. Therefore, only background noise from solar irradiation will be considered for this analysis. For a typical solar irradiation $P_{solar}$ (W/m$^2$) over horizontal and vertical field of view, $\theta_H$ and $\theta_V$, the scattered power can be written as follows:

$$P_{noise,dToF} = P_{solar} \times \rho \times 4tan\left(\frac{\theta_H}{2}\right) tan\left(\frac{\theta_V}{2}\right) \times \left(\frac{D_{lens}^2}{4}\right) \times \frac{2}{\pi} \times T_l \times T_f \times \Delta_{BW} \quad \text{Equation 11}$$

The SNR at the pixel before any further processing can then be estimated from the ratio of Equation 10 and 11. The probability of a valid detection can also be extracted for a given measurement window and optical power. This is estimated from the conditional probability that a signal event is detected, given that no noise event has been detected at a given pixel. Typically, a group of SPADs are combined to enhance this probability for a given sensor configuration.

### *C. Analytical simulations*

In order to make a quantitative comparison, a typical LiDAR system in an outdoor scenario for long range will be considered. Table 1. summarizes the list of various simulation parameters used for this comparison and Figures 4 – 6 show the simulation results.

| PARAMETER | SPAD-dToF PIXEL | COHERENT HETERODYNE PIXEL |
|---|---|---|
| Transmit power, $P_{tx}$ | Pulsed mode – 40W peak | Continuous mode – 4mW |
| Tx wavelength, λ | 905nm | 1310nm |
| Laser pulse width | ~5ns | NA |
| Chirp length, $t_{chirp}$ | NA | 32µs |
| Optical energy | 200 nJ per pulse | 128 nJ per chirp |
| Ambient light | 100 kLux | |
| Lens efficiency, $T_l$, Filter efficiency, $T_f$ | Assumed 90 % | |
| Filter bandwidth, $\Delta_{BW}$ | 20nm | NA |
| Distance, d | Up to 100m | Up to 100m |
| Number of pixels, N | 320 × 240 | 320 × 240 |
| Field of view, $\theta_H \times \theta_V$ | ~60 × 40 | ~60 × 40 |
| Lambertian reflectivity, $\rho$ | 10% | 10% |
| SPAD PDE | Assumed ~20% | NA |
| Photodiode responsivity, $R_{PD}$ | NA | 0.9 A/W |

Table 1 – Summary of the main simulation parameters for the analysis.

The single-shot SNR versus distance is plotted for a coherent heterodyne pixel and a dToF pixel on Figure 4. Three different Rayleigh ranges ($R_{max}$) are plotted to cover applications from consumer to automotive, where $R_{max}$ can reach beyond 100m. For a single shot equivalent to a chirp of 32µs in a coherent imaging pixel, the SNR remains relatively flat over the Rayleigh range, as modelled in Equation 2. This is different compared to a dToF sensor where the system SNR rolls off with $1/d^2$. For the example simulated here, an optical energy of a single pulse in a dToF (200nJ) results in an insufficient SNR with a poor detection probability (see Figures 4–5).

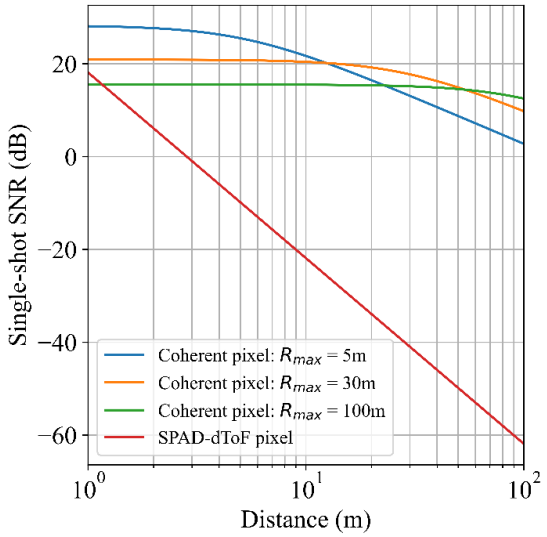


Figure 4- SNR vs. distance simulation for parameters in Table 1.

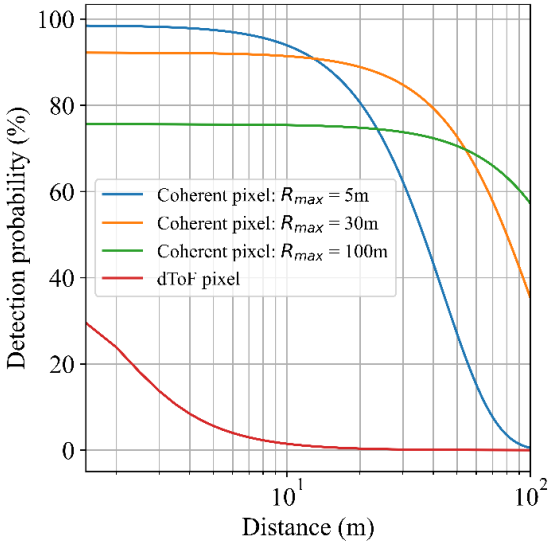


Figure 5- Detection probability (%) vs. distance simulation for parameters in Table 1.

In the presence of high ambient light, which can reach up to 100kLux in an outdoor LiDAR, a dToF histogram is typically accumulated over several laser shots, to be able to distinguish the target signal in the presence of background noise. This often comes at the expense of high optical energy, which can easily reach several µJs until a good SNR is obtained. In such cases, care must be taken to ensure that laser safety standards are not violated.
In contrast, the optical energy of a single-shot coherent pixel, although similar in magnitude (~128nJ), delivers a

significantly higher base SNR and detection probability compared to a dToF pixel, as illustrated in Figure 4–5. Moreover, the background noise does not contribute coherently in a heterodyne pixel, further enhancing its robustness in outdoor scenarios.

That said, application specific requirements and any non-ideality in the system can impose constraints on the achievable SNR and several acquisitions may need to be combined to improve SNR and detection probability, especially in long range LiDAR. This is often a system trade-off and has implications on the achievable frame rate as well. Naturally, lower frame rates imply longer integration times per chirp and/or multiple shots, resulting in higher SNR and detection probability.

## III. COHERENT LIDAR – MEASUREMENT RESULTS

This section supports the analysis in Section II with some measurement results. A high-level diagram of the setup is shown in Figure 6. A $P_{tx}$ of 0.5mW is emitted from the laser which feeds into a coherent imaging photonic integrated circuit (PIC) array via a network of optical modulator, amplifier and switches. This corresponds to an equivalent optical energy of ~16nJ for a chirp length of 32µs. Off-the-shelf optics was used in this setup.

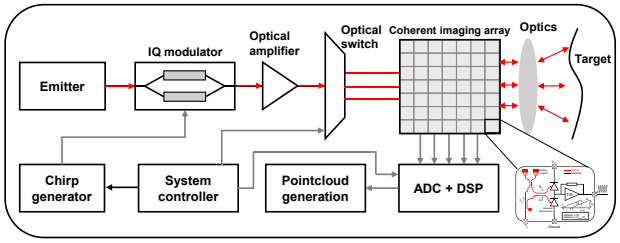


Figure 6- Block diagram of the measurement setup.

An external chirp generator on an FPGA provides the required modulation to the laser over a bandwidth of 6GHz and chirp length of 32µs. The heterodyne signal generated from the PIC array is digitized and processed using an off-chip ADC and DSP. Figure 7 shows a measurement result obtained in an indoor setup for target distance up to 10m. A dToF pixel with a comparable pulse energy is also simulated alongside.

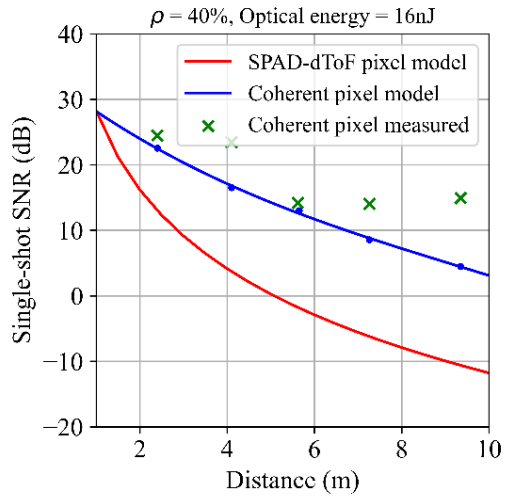


Figure 7- Measured SNR vs. distance in indoor light.

For an energy as low as 16nJ, a coherent pixel provides a relatively high base SNR, despite unoptimized optics used here for our first characterization. Currently used optics limited the collimation we could achieve, resulting in a diverging beam waist. In the future, custom optics will be developed for the final imaging system to provide a collimated beam over the Rayleigh range. In that scenario, the SNR should remain relatively flat over $R_{max}$, as estimated from the simulations shown in Section II. Figure 8 shows the measured detection probability versus SNR for different target reflectivity at ~4.5m for a single chirp. Good agreement between model (Equation 7) and measurements is found, where increasing SNR resulted in higher detection probabilities.

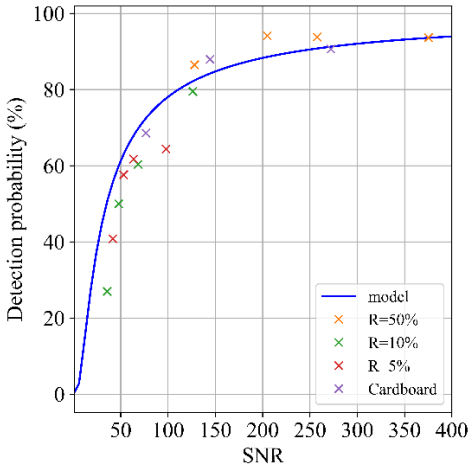


Figure 8- Measured detection probability (%) vs SNR (linear scale) for different target reflectivity (R).

## IV. CONCLUSIONS AND FUTURE OUTLOOK

In this work, we have presented and analyzed the concepts of a coherent 3D imaging pixel as a suitable technology for outdoor LiDAR. With its inherent insensitivity to background noise, such as solar irradiation, coherent detection provides a significantly higher SNR at low optical budget. Especially, where high frame rates need to be met, this is an important advantage for long range applications. Furthermore, the recent work demonstrated in [5] also shows the scalability of this approach towards a large format imaging array due to its compatibility with mass-producible CMOS technology. Future work will include custom optics development and characterization in real outdoor scenarios.

## REFERENCES


[1] Gyongy, Istvan, et al. "A direct time-of-flight image sensor with in-pixel surface detection and dynamic vision." IEEE Journal of Selected Topics in Quantum Electronics 30.1: Single-Photon Technologies and Applications (2023): 1-11.

[2] Kumagai, Oichi, et al. "7.3 A 189× 600 back-illuminated stacked SPAD direct time-of-flight depth sensor for automotive LiDAR systems." 2021 IEEE International Solid-State Circuits Conference (ISSCC). Vol. 64. IEEE, 2021.

[3] https://autonomoustuff.com/lidar-chart

[4] Tontini, Alessandro, et al. "Comparative evaluation of background-rejection techniques for SPAD-based LiDAR systems." Integration 90 (2023): 1-10.

[5] Nicolaescu, Remus, et al. "3D imaging via silicon-photonics-based LIDAR." *Silicon Photonics XVI*. Vol. 11691. SPIE, 2021.

[6] Osche GR. Optical detection theory for laser applications. 2002 Jul.